π – π orbital resonance in twisting duplex DNA: Dynamical phyllotaxis and electronic structure effects

Article *in* Physical review. B, Condensed matter · September 2009

DOI: 10.1103/PhysRevB.80.125102

CITATIONS
13

READS
115

1 author:

Enrique Macia
Complutense University of Madrid
130 PUBLICATIONS **3,188** CITATIONS

SEE PROFILE

π-π orbital resonance in twisting duplex DNA: Dynamical phyllotaxis and electronic structure effects

Enrique Maciá
Departamento de Física de Materiales, Facultad CC. Físicas, Universidad Complutense de Madrid, E-28040 Madrid, Spain
(Received 5 June 2009; revised manuscript received 23 July 2009; published 3 September 2009)

The presence of synchronized, collective twist motions of the Watson-Crick base pairs in DNA duplexes (helicoidal standing waves) can efficiently enhance the π-π orbital overlapping between nonconsecutive base pairs via a long-range, phonon-correlated tunneling effect. The resulting structural patterns are described within the framework of dynamical phyllotaxis, providing a realistic treatment which takes into account both the intrinsic three-dimensional, helicoidal geometry of DNA, and the coupling between the electronic degrees of freedom and double-helix DNA molecular dynamics at low frequencies. The main features of the resulting electronic band structures are discussed for several resonance frequencies of interest, highlighting the possible biophysical implications of the obtained results.

DOI: 10.1103/PhysRevB.80.125102 PACS number(s): 87.14.gk, 72.80.Le, 72.20.Ee, 87.15.ad

I. INTRODUCTION

When macromolecules of biological interest are considered from the viewpoint of condensed-matter physics a fundamental question naturally arises regarding the potential role of certain physical properties on their biological function. For instance, the nature of DNA-mediated charge migration has been related to the understanding of damage recognition process, protein binding, or with the task of designing nanoscale sensing of genomic mutations, opening new challenges for emerging nanobiotechnologies.[1–3] Charge migration in DNA depends on the coupling between π orbitals belonging to neighboring nucleobases stacked along the helix axis direction, which is measured in terms of the π-π orbital overlapping transfer integral, t.[4] As a first approximation transfer integral values were usually computed for idealized DNA geometries assuming that t does not significantly change with the molecular geometry during charge migration (the so-called Condon approximation). Among all possible configurations of a given base pairs (bps) stack, the so-called eclipsed one (i.e., vanishing relative twist angle between neighboring bps) exhibits the strongest electronic coupling for charge transfer [e.g., $t_*=0.372$ eV for a $(G:C)_2$ stack with an interplanar separation of 0.34 nm].[5] However, in the canonical B-DNA form, consecutive bps are twisted an angle $\theta_0 \simeq \pi/5$ at equilibrium conditions. As a result, the π-π orbital overlapping is substantially reduced as compared to that corresponding to the optimal geometrical configuration [e.g., $t=0.047$ eV for the previously considered $(G:C)_2$ stack in this case].[5] In addition, at physiological temperatures the relative orientation of neighboring bases becomes a function of time due to thermal fluctuations, thereby modifying their mutual overlapping in an oscillatory way. Accordingly, the electronic coupling between nucleobases is very sensitive to structural fluctuations and the Condon approximation is rather limited.[6–8]

Making use of molecular-dynamics calculations it was shown that the standard deviation of the nucleobases coupling is much larger than its average value. This result indicates that charge transport in DNA preferentially occurs in specific conformations, which may considerably deviate from the canonical B-DNA structure.[9] In fact, recent studies have revealed that transfer integral values are extremely sensitive to conformational fluctuations, so that the transport efficiency calculated ignoring dynamical effects can be underestimated by several orders of magnitude.[5,10] Thus, depending on the DNA sequence composition, its length and effective temperature, reported transfer integral values can vary over a relatively broad interval, ranging from $t=0.01$ to $t=0.4$ eV.[6,11–21] These figures imply charge migration time scales within the range $\hbar/t \simeq 2-66$ fs for coherent tunneling. Nevertheless, femtosecond spectroscopy experiments aimed at determining the rates of DNA charge-transport processes unveiled a two-step decay process with characteristic time scales of 5–10 and 75 ps, respectively,[22,23] which cannot be accounted for in terms of coherent tunneling processes alone. The 75-ps time scale is about one order of magnitude larger than the typical figure for lattice or intramolecular dynamical degrees of freedom, and may probably be related to the presence of localized electronic states undergoing thermally induced hopping migration. On the other hand, it has been suggested that the 5–10-ps time scale could be related to an electron-phonon coupling mechanism between the electronic degrees of freedom and molecular vibrations, thereby resulting in a substantial reduction in the coherent tunneling time scale from fs to ps. Nonetheless, a detailed physical scenario describing such a proposed mechanism is still missing.

Over the longest (ns) time scales currently accessible by full atomistic modular dynamics simulations the double-helix undergoes large-scale global oscillatory motions dominated by rise and twist oscillations of the bp planes as a whole.[24] In particular, typical fluctuation angles for twist modes are about $5-10°$ in the ps to ns time window. These motions dominate the range of molecular conformations generated by thermal agitation and are most relevant to any biological process which relies on *shape recognition*. The role of thermal fluctuations on the charge-transfer efficiency has been discussed in a number of previous works where these fluctuations are treated by sampling the initial angular velocities and twist angles from a Boltzmann distribution at a given temperature.[19,20,25–30] These works dealt with oversim-

plified spatial structures, where DNA chain is described in terms of effective linear (one-dimensional) or ladderlike (two-dimensional) models.[31] Subsequently, the combined effect of helical structure and bps twist motion on charge transfer through more realistic duplex DNA at low temperatures was considered.[32] The physical picture emerging from that work was that although an ensemble of bps twisting back and forth around the helix axis generally results in a degraded charge-transfer efficiency, a significant improvement of charge migration can occur via charge coupling to certain lattice modes at low temperatures, in line with several works suggesting that structural fluctuations may facilitate charge transfer in DNA.[9,33,34] In fact, recent quantum-mechanics/molecular-dynamics studies of a duplex $(GT)_{15}$ oligomer have shown the presence of large fluctuations of t^2 (the magnitude determining the charge-transfer rate) about one order of magnitude larger than the averaged $\langle t^2 \rangle$ value, occurring every 1 ps on the average.[5] Following this approach, a systematic study of those π stack conformations leading to higher mobilities has been performed for several DNA duplex oligomers.[10] However, the analysis of the obtained molecular-dynamics snapshots does not provide a clear enough picture on the spatial stack structures showing the best hole mobility. Accordingly, some complementary approaches would be welcome in order to get a more detailed picture of the optimal DNA stack configurations.[5,6,11]

Spurred by these results, in the present work we shall study the physical role of collective twist motions of the bps which occur in a synchronized manner, giving rise to the emergence of helicoidal standing waves in the DNA duplex. The resulting structural patterns will be described in the framework of dynamical phyllotaxis, by focusing on the presence of long-range spatial correlation effects mediated by twist phonons coupling. Though strictly speaking phyllotaxis is a botanical issue,[35] in a wider sense, the notion of phyllotaxis can be applied to a variety of physical systems that exhibit a self-organization very similar to a botanical one, like Bernard convection cells,[36] or vortex lattices in superconductors.[37] In these systems the emergence of phyllotactic patterns can be studied under controlled situations by mimicking the growth conditions in a plant. To this end, basic botanical elements were treated as pointlike particles interacting through a repulsive potential and their location was determined by calculating the total energy due to all the previous ones, then placing the new element at the point of minimum energy.[38] Accordingly, these results suggest that phyllotaxis may be a general phenomenon in soft lattices composed of interacting subsystems under strong deformation conditions. Quite remarkably, these conditions are fulfilled by DNA chains as we will show in the present work. In this way, we disclose the relationships between a number of π-π overlapping resonance frequencies and the main features of the resulting DNA electronic band structure, providing a realistic treatment which takes into account (i) the intrinsic three-dimensional, helicoidal geometry of DNA, and (ii) the coupling between the electronic degrees of freedom and (low frequency) duplex DNA molecular dynamics.

II. DNA MODEL DESCRIPTION

Two kinds of order coexist in biological DNA, each one related to two separate subsystems in the DNA helix, namely, the nucleobase system and the backbone system.[39–41] Thus, one has periodic structural order at the *atomic scale* in the sugar-phosphate backbone, yielding discrete Bragg spots in x-ray diffraction patterns, which exhibit a characteristic St. Andrew's cross-shaped pattern. On the other hand, one has aperiodic, informative chemical order at the *molecular scale*, as determined by the sequence of Watson-Crick bps. The chemical order of the bps sequence can be properly characterized by *ab initio* quantum chemistry calculations, which properly highlight the emergence of molecular orbitals beyond the atomic scale. In order to describe the nucleobase system electronic structure, defining most basic properties of DNA molecule, we must consider a model Hamiltonian accounting for different scales of time and energy by means of an adequate choice of generalized coordinates describing both electronic and dynamic DNA degrees of freedom. Thus, effective model Hamiltonians can be expressed as the sum of two main contributions $H=H_e+H_l$, where H_e describes the charge dynamics over the π-stacked electronic system and H_l describes the duplex DNA dynamics. The electronic degrees of freedom of a double-stranded DNA (including sugar-phosphate and environmental effects) are described in terms of the effective Hamiltonian,[32,42,43]

$$H_e = \sum_{n=1}^{N} \tilde{\varepsilon}_n(E) c_n^{\dagger} c_n - \sum_{n=1}^{N-1} t(\theta_{n,n+1})(c_n^{\dagger} c_{n+1} + c_{n+1}^{\dagger} c_n), \quad (1)$$

where $c_n^{\dagger}$ (c_n) is the creation (annihilation) operator for a charge at nth site, and N is the number of bps. Equation (1) describes the charge propagation through a DNA duplex in terms of an equivalent one-dimensional lattice, where the renormalized "atoms" correspond to complementary pairs in the original DNA molecule whose on-site energies $\tilde{\varepsilon}_n(E) \in \{\alpha(E), \beta(E)\}$ depend on the charge energy E and enclose the quantum description of the Watson-Crick bp energetics through the expressions[42,43]

$$\alpha(E) = \alpha_0 + \alpha_1 E + \frac{2t_b^2}{E-\gamma}, \quad \beta(E) = \beta_0 + \beta_1 E + \frac{2t_b^2}{E-\gamma}, \quad (2)$$

with $\alpha_0 \equiv a_0 - \gamma\alpha_1$, $\beta_0 \equiv b_0 - \gamma\beta_1$, $a_0 \equiv t_{GC} + 2(\varepsilon_G + \varepsilon_C)$, $b_0 \equiv t_{AT} + 2(\varepsilon_A + \varepsilon_T)$, $\alpha_1 \equiv (\varepsilon_G^2 + \varepsilon_C^2)/t_b^2$, and $\beta_1 \equiv (\varepsilon_A^2 + \varepsilon_T^2)/t_b^2$, where $t_{GC(AT)}$ describes the hydrogen bonding between the complementary bases, ε_k are the nucleobases on-site energies, t_b describes the transfer integral between backbone and base states, and γ accounts for the sugar-phosphate backbone on-site energies, generally depending on the presence of water molecules and counterions attached to the backbone. Finally, the parameter $t(\theta_{n,n+1})$ describes the π-π overlapping transfer integral, where $\theta_{n,n+1}$ measures the relative angular displacement between two adjacent bps around the helix axis. For small enough twists this transfer integral can be approximated as[32]

$$t(\theta_{n,n\pm1}) \simeq t_0(1 - \chi|\theta_{n,n\pm1}|^2), \quad (3)$$

where t_0 is the transfer integral value corresponding to the eclipsed geometry (i.e., $\theta_n \equiv 0$) and the dimensionless parameter $\chi \equiv \bar{\eta}(R_0/l_0)^2 > 0$ measures the coupling strength be-

TABLE I. Parameters adopted for the effective Hamiltonian considered in this work. Electronic Hamiltonian parameters are arranged in order to illustrate the different energy scales of relevance in the DNA system (in eV) (Refs. 42 and 43). Nucleotides masses (including nucleobase, sugar and phosphate group masses) are expressed in u.m.a. units. Sugar-phosphate backbone elastic constant k and charge-lattice coupling coefficient χ values taken from Ref. 46 and Ref. 47, respectively.

Model Hamiltonian parameters
$\gamma=12.27$
$\varepsilon_G=7.77$, $\varepsilon_C=8.87$
$\varepsilon_A=8.25$, $\varepsilon_T=9.13$
$t_b=1.5$, $t_0=0.15$
$t_{GC}=0.90$, $t_{AT}=0.34$
$m_G=347.05$, $m_C=307.05$
$m_A=331.06$, $m_T=322.05$
$k=0.014$ eV Å^{-2}
$\chi=2.92$

tween the charge and the lattice system, where $R_0 \simeq 1$ nm is the B-DNA equilibrium radius, $l_0=\sqrt{h_0^2+4R_0^2\sin^2(\theta_0/2)} \simeq 0.7$ nm, is the equilibrium distance between neighboring bases along the helical strand, $h_0 \simeq 0.34$ nm is the equilibrium separation between two successive bp planes along the helix axis, and $\bar{\eta} \equiv 1+|\eta_{pp\pi}|/\eta_{pp\sigma}$, where $\eta_{pp\pi}$ and $\eta_{pp\sigma}$ describe the hybridization matrix elements between neighboring bases p_z orbitals.[4] Equation (3) generalizes the function adopted in some previous works, which implicitly assumed $\chi=1/2$ (i.e., $t \simeq t_0 \cos\theta_{n,n\pm1}$).[25,27,28,44,45]

When describing the phonon dynamics in DNA one can disregard the inner degrees of freedom of the bases, since we can separate the fast vibrational motions of atoms about their equilibrium positions from the slower motions of molecular groups. In this work we shall focus on the low-frequency dominant twist mode, hence keeping the DNA radius constant. In that case, one can express the lattice Hamiltonian in the form[32]

$$H_l=\frac{1}{2\xi^2}\sum_{n=1}^{N}\frac{p_n^2}{m_n}+4k\sum_{n=1}^{N-1}\left(\sqrt{c^2\phi_{n,n+1}^2+R_0^2\sin^2\phi_{n,n+1}}-\frac{l_0}{2}\right)^2, \tag{4}$$

where $\xi \equiv \sqrt{R_0^2+c^2}$, $c=h_0/\theta_0$, m_n is the bp mass, p_n is the angular momentum, k is the effective force constant upon distortion of the sugar-phosphate backbone, and $\phi_{n,n+1} \equiv \theta_{n,n+1}/2$. From data listed in Table I one realizes that, though the masses of the four nucleotides are different, when paired according to Chargaff's rule one gets $m_G+m_C \simeq m_A+m_T \simeq 653.5 \pm 0.5$. Accordingly, one can safely assume a common value for *all the bps* in the chain (i.e., $m_n=2\mu\ \forall n$, with $\mu \simeq 326.75$ u.m.a.). This remarkable symmetry nicely illustrates the significant role of the chemically based Chargaff's rule in the physical, dynamical behavior of DNA chains.[48] The low-frequency dynamical response is obtained linearizing the canonical equations of motion derived from Eq. (4) by considering only linear terms to obtain,[32]

$$\ddot{\theta}_{n,n+1}-\ddot{\theta}_{n,n-1}=\omega_0^2(\theta_{n+1,n+2}-3\theta_{n,n+1}+3\theta_{n,n-1}-\theta_{n-1,n-2}), \tag{5}$$

where $\omega_0 \equiv \sqrt{k/\mu}$ is the natural twist frequency of each bp ($\omega_0 \simeq 6.4\times10^{11}$ rad/s; $T_0 \equiv 2\pi/\omega_0 \simeq 9.8$ ps). Equation (5) describes a *correlated* motion involving three consecutive bps (codon unit). Searching for solutions in the form of linear waves we plug the ansatz $\theta_{n,k}=\sqrt{2}\theta_0 e^{i\omega t}\cos(\lambda_{n,k}q)$, where q is the wave number and $\lambda_{n,k} \equiv (n+k)l_0/2$ measures the correlation length between bps in l_0 units, into Eq. (5) to obtain the previously reported dispersion-relation $\omega^2=4\omega_0^2\sin^2(ql_0/2)$.[46] Physically, this ansatz can be regarded as describing the superposition of two waves of the form $\sqrt{2}\theta_0 e^{i(\omega t \pm q\lambda_{n,k})}/2$ propagating in opposite sense along the DNA chain. Thus, we are considering stationary patterns related to helical standing waves resulting from the superposition of orchestrated twist oscillations propagating back and forth the DNA chain.

Making use of $\theta_{n,k}$ into Eq. (3) one can express the Schrödinger equation corresponding to Eq. (1) in the form

$$[E-\tilde{\varepsilon}_n(E)]\psi_n-\tau_0(\psi_{n+1}+\psi_{n-1})+B[\psi_{n+1}T_{2n+1}(\Omega)+\psi_{n-1}T_{2n-1}(\Omega)]=0, \tag{6}$$

where $\tau_0 \equiv t_0(1-\chi\theta_0^2)$, $B \equiv t_0\chi\theta_0^2$, and $T_k(\Omega) \equiv \cos(k\cos^{-1}\Omega)$ are Chebyshev polynomials of the first kind with $\Omega \equiv 1-\omega^2/2\omega_0^2$ ($\Omega \in [-1,1]$). The first two terms in Eq. (6) describe the charge dynamics (including helical geometry effects along with a complete account of nucleotide energetics) in the standard tight-binding form. The last term in Eq. (6) describes charge-lattice dynamical effects. In order to clearly grasp the physics underlying Eq. (6) it is convenient to properly rewrite this last term. To this end, we make use of the multiplication formula $T_{k+l}=T_kT_l-(1-\Omega^2)U_{k-1}U_{l-1}$, where $U_{k-1}(\Omega) \equiv \sin(k\cos^{-1}\Omega)/\sqrt{1-\Omega^2}$ are Chebyshev polynomials of the second kind, along with the functional equations $T_{2k}(\Omega)=T_k(2\Omega^2-1)$ and $U_{2k-1}(\Omega)=2\Omega U_{k-1}(2\Omega^2-1)$. In this way, taking into account the relationships $T_{\pm1}(\Omega)=\Omega$, $U_0(\Omega)=1$, and $U_{-2}(\Omega)=-1$, we can express

$$T_{2n\pm1}(\Omega)=\Omega[T_n(\tilde{\Omega}) \mp (1-\tilde{\Omega})U_{n-1}(\tilde{\Omega})], \tag{7}$$

where $\tilde{\Omega} \equiv 2\Omega^2-1$ ($\tilde{\Omega} \in [-1,1]$). Finally, making use of the recurrence relations

$$U_n(x)-xU_{n-1}(x)-T_n(x)=0,$$

$$T_n(x)-xU_{n-1}(x)+U_{n-2}(x)=0, \tag{8}$$

in Eq. (7), we get

$$T_{2n\pm1}(\Omega) \equiv \Omega g_{n,n\pm1}(\tilde{\Omega}), \tag{9}$$

with,

$$g_{n,n+1}(\tilde{\Omega})=U_n(\tilde{\Omega})-U_{n-1}(\tilde{\Omega}), \tag{10}$$

$$g_{n,n-1}(\tilde{\Omega}) = U_{n-1}(\tilde{\Omega}) - U_{n-2}(\tilde{\Omega}). \quad (11)$$

Thus, we can rewrite Eq. (6) in the standard tight-binding form

$$[E - \tilde{\varepsilon}_n(E)]\psi_n - \tilde{\tau}_{n,n+1}(\omega)\psi_{n+1} - \tilde{\tau}_{n,n-1}(\omega)\psi_{n-1} = 0, \quad (12)$$

where

$$\tilde{\tau}_{n,n\pm1}(\omega) \equiv t_0\{1 - \chi\theta_0^2[1 + \Omega g_{n,n\pm1}(\tilde{\Omega})]\}, \quad (13)$$

with

$$\Omega = \frac{2\omega_0^2 - \omega^2}{2\omega_0^2}, \quad \tilde{\Omega} = \frac{[(2+\sqrt{2})\omega_0^2 - \omega^2][(2-\sqrt{2})\omega_0^2 - \omega^2]}{2\omega_0^4}. \quad (14)$$

Equation (12) contains detailed information about the electronic structure of the double-helix in terms of the energy dependent on-site energies $\tilde{\varepsilon}_n(E)$ given by Eq. (2) along with the frequency dependent transfer integrals $\tilde{\tau}_{n,n+1}(\omega)$ given by Eq. (13). These transfer integrals describe a π-π overlapping modulation between successive bps which depends on the twist frequency value. Accordingly, for each considered frequency ω one obtains a specific distribution of transfer integrals values through the chain resulting from the charge-lattice coupling. The simplest possible distribution corresponds to the resonance frequency $\omega_* = \sqrt{2}\omega_0$ ($\Omega = 0$, $\tilde{\Omega} = -1$), for which we obtain the homogeneous distribution $\tilde{\tau}_{n,n+1}(\omega_*) = \tau_0$ $\forall n$. The dispersion relation yields the wavelength value $\lambda_* = 4l_0$ in this case, hence indicating that the period of the corresponding helical standing wave extends over five bps along the DNA backbone (i.e., half a period of the B-DNA unit cell containing 10 bps). Similarly simple $\tilde{\tau}_{n,n+1}(\omega)$ distributions are obtained for the frequency spectrum band edges $\omega_- = 0$ ($\Omega = 1$, $\tilde{\Omega} = 1$) and $\omega_+ = 2\omega_0$ ($\Omega = -1$, $\tilde{\Omega} = 1$). In fact, keeping in mind the relationship $U_n(1) = n + 1$ in Eq. (10), one gets $g_{n,n+1}(1) = 1$ $\forall n$, so that we obtain the homogeneous distributions $\tau_{n,n+1}(\omega_+) = t_0 \equiv a$, and $\tau_{n,n+1}(\omega_-) = t_0(1 - 2\chi\theta_0^2) \equiv b$ $\forall n$, from Eq. (13). The frequency ω_- (with $\lambda_- = l_0$) describes the shortest helical standing wave, comprising just two consecutive bps in its period length. On the other hand, the frequency ω_+ (with $\lambda_+ = 2l_0$) describes a helical standing wave spreading over three consecutive bps forming a typical codon unit.

III. LONG-RANGE CORRELATED RESONANCE EFFECTS

The physical picture inspiring the following approach is based on the fact that the presence of collective, orchestrated twist motions around the DNA helix axis can efficiently enhance the π-π orbital overlapping between bps which *are not* necessarily close to each other *along the backbone* chain, hence promoting charge transfer via a long-range, *phonon-correlated* tunneling effect. This property is intimately related to the helical geometry of the nucleobases arrangement along the duplex chain and expresses the fact that their order of appearance (n label) does not always coincide with the relative values of their metric distance to each other. This important feature is illustrated in Fig. 1(a), where we see that the distance between nucleotides n and $n+3$ is *shorter* than that between the consecutive nucleotides n and $n+1$. Under appropriate resonance conditions this local feature, involving a relatively small number of neighboring nucleotides, extends over the entire DNA chain as a consequence of the structural periodicity of the resulting helical standing wave. Figure 1(b) schematically depicts the relative positions of a series of successive bps for a typical wave. The bps dimer labeled A represents two optimally orientated bps attaining a large π-π orbital overlapping. Due to the twist modulation, successive bps will progressively separate from this optimal configuration (B), eventually reaching the worst one (C), then progressively twisting back (D), to finally reach the optimal overlap configuration again (E). The distance between both optimally twist matched bps dimers A and E defines the standing-wave correlation length, which is conveniently measured by the number of intervening bps, m. The resonance condition then requires that the dimers A and E will share the same transfer integral value for a given frequency value ω. Such a requirement can be mathematically expressed in the form $\tilde{\tau}_{n,n+1}(\omega) = \tilde{\tau}_{n+m,n+1+m}(\omega)$, where n denotes an arbitrary position along the chain. According to Eq. (13) the condition above reduces to $g_{n,n+1} = g_{n+m,n+1+m}$, which after Eq. (10) leads to $U_n(\tilde{\Omega}) - U_{n-1}(\tilde{\Omega}) = U_{n+m}(\tilde{\Omega}) - U_{n+m-1}(\tilde{\Omega})$. Then, making use of the relationships $U_{n+m}(x) = U_n(x)T_m(x) + T_{n+1}(x)U_{m-1}(x)$, and $U_{m+n-1}(x) = U_{m-1}(x)T_n(x) + T_m(x)U_{n-1}(x)$, the long-range resonance condition reads

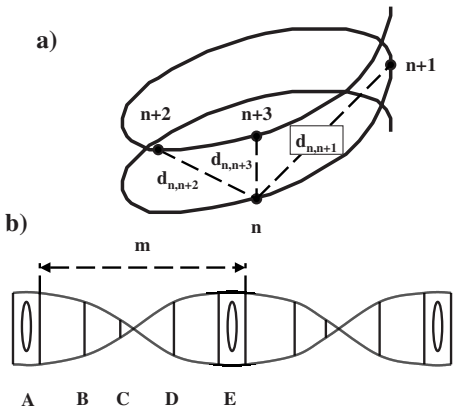

FIG. 1. (a) Arbitrary sequence of three consecutive nucleotides along a helical path whose metric distances satisfy the relationship $d_{n,n+3} < d_{n,n+2} < d_{n,n+1}$. (b) Sketch showing a characteristic duplex DNA helical standing-wave pattern. The vertical lines depict the cross-section projections of each bp along the helix axis, their length providing a measure of their twist magnitude. Thick lines represent the sugar-phosphate profile. Optimally π-π overlapping bps are indicated by the presence of the ovals. m measures the π-π overlapping resonance correlation length. For more details see the text.

$$(T_m - 1)(U_n - U_{n-1}) + U_{m-1}(T_{n+1} - T_n) = 0, \quad (15)$$

where for the sake of clarity we have dropped out the argument dependence of the Chebyshev polynomials on the vari-

TABLE II. The resonance conditions given by Eq. (17), properly factorized in terms of Chebyshev polynomials $U_k(\tilde{\Omega})$ and $T_k(\tilde{\Omega})$, are listed along with their related frequency values solutions for the correlation length values $m=1-6$. The presence of $\tau \equiv (1+\sqrt{5})/2$ (the so-called golden mean) is directly related to the decagonal symmetry of the B-DNA equilibrium configuration with respect to its helical axis. For more details see the text.

m	Equation (17)	$\tilde{\Omega}$	Ω	ω/ω_0	m	Equation (17)	$\tilde{\Omega}$	Ω	ω/ω_0
1	$(\tilde{\Omega}-1)U_n=0$	± 1	$0,\pm 1$	$0,2,\sqrt{2}$	2	$T_{n+2}=T_{n+1}$	1	± 1	0,2
3	$(\tilde{\Omega}-1)(2\tilde{\Omega}+1)U_{n+1}=0$	± 1	$0,\pm 1$	$0,2,\sqrt{2}$	4	$\tilde{\Omega}(T_{n+3}-T_{n+2})=0$	1	± 1	0,2
		$-\frac{1}{2}$	$\pm\frac{1}{2}$	$1,\sqrt{3}$			0	$\pm\frac{\sqrt{2}}{2}$	$\sqrt{2\pm\sqrt{2}}$
5	$(\tilde{\Omega}-1)(4\tilde{\Omega}^2+2\tilde{\Omega}-1)U_{n+2}=0$	± 1	$0,\pm 1$	$0,2,\sqrt{2}$	6	$(4\tilde{\Omega}^2-1)](T_{n+4}-T_{n+3})=0$	1	± 1	0,2
		$-\frac{\tau}{2}$	$\pm\frac{\tau^{-1}}{2}$	$\tau,\sqrt{1+\tau^{-2}}$			$-\frac{1}{2}$	$\pm\frac{1}{2}$	$1,\sqrt{3}$
		$\frac{\tau^{-1}}{2}$	$\pm\frac{\tau}{2}$	$\tau^{-1},\sqrt{1+\tau^2}$			$+\frac{1}{2}$	$\pm\frac{\sqrt{3}}{2}$	$\sqrt{2\pm\sqrt{3}}$

able $\tilde{\Omega}$. By properly combining Eqs. (8) one obtains

$$T_{n+1}-T_n=(\tilde{\Omega}-1)(U_n+U_{n-1}), \tag{16}$$

so that one can express Eq. (15) in the more convenient form

$$(U_m-U_{m-1}-1)U_n+(1-U_{m-1}+U_{m-2})U_{n-1}=0. \tag{17}$$

In this way, by fixing the correlation length value m, the resonance condition $\tilde{\tau}_{n,n+1}(\omega)=\tilde{\tau}_{n+m,n+1+m}(\omega)$ is expressed in terms of a relationship involving Chebyshev polynomials of the second kind which can be solved in order to determine the corresponding frequency values. In the trivial case $m=1$, Eq. (17) reduces to $2(\tilde{\Omega}-1)U_n(\tilde{\Omega})=0\ \forall n$, which leads to the solutions $\tilde{\Omega}=\pm 1\Rightarrow\Omega=\{0,\pm 1\}$. These solutions correspond to the frequencies $\omega_*=\sqrt{2}\omega_0$, $\omega_-=0$, and $\omega_+=2\omega_0$, previously discussed in Sec. II. In the case $m=2$, making use of Eq. (8) along with the recursion relation $U_{n+1}(x)-2xU_n(x)+U_{n-1}(x)=0$, Eq. (17) becomes $2(\tilde{\Omega}-1)(U_{n+1}+U_n)=0$, which, according to Eq. (16), is equivalent to the condition $T_{n+2}(\tilde{\Omega})=T_{n+1}(\tilde{\Omega})\ \forall n$, leading to the solutions $\tilde{\Omega}=1\Rightarrow\Omega=\{\pm 1\}$. Thus, the solution $\Omega=0$, corresponding to the resonance frequency ω_*, is not allowed in this case. In the case $m=3$, Eq. (17) can be expressed in the form $(\tilde{\Omega}-1)(2\tilde{\Omega}+1)U_{n+1}(\tilde{\Omega})=0\ \forall n$, leading to the solutions $\tilde{\Omega}=\{\pm 1,-\frac{1}{2}\}\Rightarrow\Omega=\{0,\pm 1,\pm\frac{1}{2}\}$. Therefore, we get additional values corresponding to the frequencies $\omega_3^-\equiv\omega_0$ and $\omega_3^+\equiv\sqrt{3}\omega_0$. Making use of Eq. (10) one has $g_{n,n+1}(-\frac{1}{2})=2\cos[(2n+1)\pi/3]$, so that we get two possible transfer integral values $\tau_{n,n+1}(\omega_3^-)=t_0(1-3\chi\theta_0^2/2)\equiv c$ and $\tau_{n,n+1}(\omega_3^+)=t_0(1-\chi\theta_0^2/2)\equiv d$.

Analogously proceeding we can obtain the resonant frequencies for any arbitrary value of the correlation length. In Table II the results corresponding to the values $m=1$ to $m=6$ are explicitly listed. By inspecting this table several conclusions can be drawn. In the first place, the different resonance configurations can be classified according to the correlation length *parity* in a natural way. Thus, all even solutions share the value $\tilde{\Omega}=1$ (i.e., ω_- and ω_+) stemming from the condition $T_k(\tilde{\Omega})=T_{k+1}(\tilde{\Omega})\ \forall k$, whereas all the odd solutions share the values $\tilde{\Omega}=\pm 1$ (i.e., ω_*, ω_-, and ω_+) stemming from the condition $U_k(\tilde{\Omega})=0\ \forall k$. In addition to these common solutions one also gets some specific frequency values for each $m>2$ value, which are determined by the presence of certain polynomial factors in Eq. (17). The transfer integral values corresponding to these specific frequencies are listed in Table III. We note that some of these specific frequencies can be shared by several m values, depending on the existence (or not) of common prime factors among the considered m values (for instance, $\omega_3^{\pm}$ frequencies appear for both $m=3$ and $m=6$). We also note that, as the value of the correlation length is progressively increased the number of available specific frequencies also grows. Therefore, the dynamical complexity arising from charge-lattice coupling effects is directly related to the relative importance of long-range correlation effects in DNA duplexes.

For each frequency listed in Table III one has a specific DNA spatial configuration resulting from its related helical standing wave. In order to visualize the corresponding patterns we will assume that, for small enough relative displacements, the Euclidean distance between two neighboring bases can be expressed as $d_{n,n\pm 1}(\omega)\simeq\xi\theta_{n,n\pm 1}(\omega)$.[32] Making use of the basic relationship $d_{n,n\pm 1}^2\simeq h_{n,n\pm 1}^2+R_0^2\theta_{n,n\pm 1}^2$, along with Eq. (9), one gets $h_{n,n\pm 1}(\omega)=h_0\sqrt{1+\Omega g_{n,n\pm 1}(\tilde{\Omega})}$, and $\theta_{n,n\pm 1}(\omega)=\pm\theta_0\sqrt{1+\Omega g_{n,n\pm 1}(\tilde{\Omega})}$. In Table IV we list the geometrical parameters of interest for each resonance frequency. On the other hand, Eq. (13) can be rewritten in the form

$$\tilde{\tau}_{n,n\pm 1}(\omega)=t_0\left(1-\frac{\chi}{c^2}h_{n,n\pm 1}^2(\omega)\right). \tag{18}$$

Since χ takes on positive values, the sign of $\tilde{\tau}_{n,n\pm 1}(\omega)$ is determined by the value of the bp interplanar distance $h_{n,n\pm 1}(\omega)$. Only when such a distance is small enough one obtains positive values for the transfer integrals, otherwise $\tilde{\tau}_{n,n\pm 1}$ takes on negative values. Accordingly, favorable (unfavorable) overlapping conditions are related to positive (negative) values of the transfer integrals, respectively. In fact, by inspecting Tables III and IV we see that the largest positive value of $\tilde{\tau}_{n,n+1}$ (labeled k) is obtained for a very tight configuration of neighboring bps, whereas such bps are quite distant from one another in the configuration corresponding to the largest negative value of $\tilde{\tau}_{n,n+1}$ (labeled b). For inter-

TABLE III. Periods of the resonance frequencies and transfer integral values given by Eq. (13) for different resonance frequencies. The estimated $\tilde{\pi}(\omega)$ values listed in the last column are obtained by adopting the model parameter values listed in Table I. For more details see the text.

m	ω label	ω/ω_0	T (ps)	$\tilde{\tau}$ label	$\tilde{\pi}(\omega)/t_0$	$\tilde{\pi}(\omega)$ (eV)
1–5	ω_+	2	4.9	a	1	+0.150
1, 3, 5	ω_*	$\sqrt{2}$	6.9	τ_0	$1-\chi\theta_0^2$	−0.023
1–5	ω_-	0		b	$1-2\chi\theta_0^2$	−0.196
3	ω_3^-	1	9.8	c	$1-\frac{3}{2}\chi\theta_0^2$	−0.109
3	ω_3^+	$\sqrt{3}$	5.7	d	$1-\frac{1}{2}\chi\theta_0^2$	+0.063
4	ω_4^+	$\sqrt{2+\sqrt{2}}$	5.3	e	$1-\frac{2-\sqrt{2}}{2}\chi\theta_0^2$	+0.099
4	ω_4^-	$\sqrt{2-\sqrt{2}}$	12.8	f	$1-\frac{2+\sqrt{2}}{2}\chi\theta_0^2$	−0.145
5	$\omega_{5,1}^-$	$\sqrt{1+\tau^2}$	5.1	g	$1-\frac{\tau^2}{2}\chi\theta_0^2$	−0.076
5	$\omega_{5,1}^+$	τ^{-1}	15.9	h	$1-\frac{3-\tau}{2}\chi\theta_0^2$	+0.031
5	$\omega_{5,2}^+$	$\sqrt{1+\tau^{-2}}$	8.3	k	$1-\frac{2-\tau}{2}\chi\theta_0^2$	+0.117
5	$\omega_{5,2}^-$	τ	6.1	l	$1-\frac{2+\tau}{2}\chi\theta_0^2$	−0.163

mediate $\tilde{\tau}_{n,n+1}(\omega)$ values one correspondingly obtains intermediate packing degrees.

Making use of the geometrical data listed in Table IV the main features of several helical standing waves are illustrated in Figs. 2–4. By properly combining the information contained in both the cross-section and axial projection views shown in these figures one can generate a cylindrical lattice where each nucleobase plays the role usually ascribed to the distribution of botanical elements (primordia, leaves) over the plant stem in botanical studies of phyllotaxis. In this way, for every standing wave characterized by its resonance frequency, we obtain a specific *DNA phyllotactic pattern*, describing the helical arrangement of the nucleobases along the duplex chain.

By inspecting Fig. 2 one sees that the helical pattern corresponding to the frequency $\omega_3^-=\omega_0$ is considerably simpler than that corresponding to the frequency $\omega_3^+\equiv\sqrt{3}\omega_0$. The spatial period of the standing wave corresponding to ω_3^+ ($P=10$ bps, $H/H_0=0.989$) is slightly shorter than that corresponding to the B-DNA unit cell in its equilibrium configuration, $H_0=3.4$ nm, whereas the period of the standing wave corresponding to ω_3^- ($P=6$ bps, $H/H_0=0.489$) is even shorter than $H_0/2$. We note that the frequency ω_3^- coincides with a single bp natural frequency ω_0, so that we also have a mechanical resonance condition in this particular case, leading to the singular configuration of collapsing bps dimers (i.e., $h_{n,n+1}=0$) at certain locations (e.g., $n=0,3,6,\ldots,$). Accordingly, this is not a representative physical instance of the kind of standing waves we are interested in. The helical pat-

TABLE IV. Geometrical parameters defining the helical standing waves shown in Figs. 2–4. For more details see the text.

$\tilde{\tau}$	$\tilde{\tau}_{n,n+1}(\omega)$ (eV)	$\sqrt{1+\Omega g_{n,n+1}}$	$h_{n,n+1}$ (nm)	$\theta_{n,n+1}$ (deg)
b	−0.196	$\sqrt{2}$	0.481	50.9
l	−0.163	$\sqrt{\frac{2+\tau}{2}}$	0.457	48.4
f	−0.145	$\sqrt{\frac{2+\sqrt{2}}{2}}$	0.444	47.0
c	−0.109	$\sqrt{3/2}$	0.416	44.1
g	−0.076	$\frac{\tau}{\sqrt{2}}$	0.389	41.2
h	+0.031	$\sqrt{\frac{3-\tau}{2}}$	0.283	29.9
d	+0.063	$\sqrt{\frac{1}{2}}$	0.240	25.5
e	+0.099	$\sqrt{\frac{2-\sqrt{2}}{2}}$	0.184	19.5
k	+0.117	$\sqrt{\frac{2-\tau}{2}}$	0.149	15.7

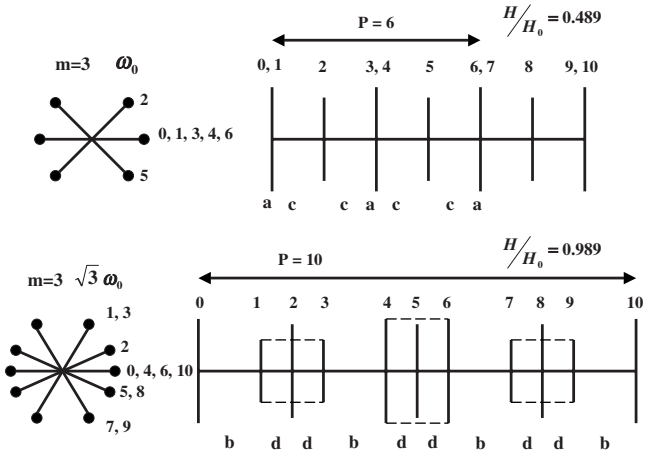

FIG. 2. Axial projection (on the left) and cross-section projection (on the right) of the helical standing waves corresponding to the frequencies $\omega_3^-=\omega_0$ and $\omega_3^+=\sqrt{3}\omega_0$ for a resonance correlation length $m=3$. For the sake of clarity the small circles (representing the nucleotides) are not included in the cross-section view. The bps interplanar distances $h_{n,n+1}$ and the relative twist angles $\theta_{n,n+1}$, corresponding to the successively numbered bps, are listed in Table IV. The numbers indicate the order of appearance of successive nucleotides along the helical strand. The letters label the different transfer integral values listed in Table III. The period of the helical standing wave is measured by P (in bps), H is its length along the helical axis and $H_0=10h_0$ is the axial length of the B-DNA form unit cell in equilibrium. For more details see the text.

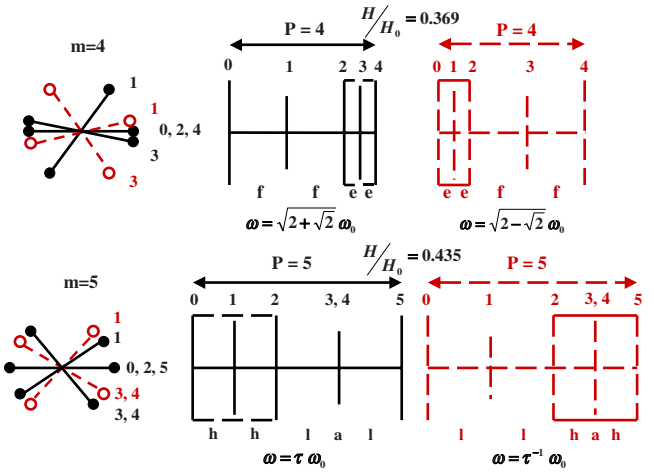

FIG. 3. (Color online) The same as Fig. 2 for the frequencies $\omega_4^{\pm}=\sqrt{2\pm\sqrt{2}}\omega_0$ (top panel) and $\tau^{\pm 1}\omega_0$ (low panel) for resonance correlation lengths $m=4$ and $m=5$, respectively. For more details see the text.

tern corresponding to the frequency $\omega_3^+\equiv\sqrt{3}\omega_0$, on the contrary, nicely illustrates the main feature stemming from the phonon-correlated orbital overlapping resonance. This feature is highlighted by the horizontal dashed lines connecting the bps labeled 1–3, 4–6, and 7–9 in the bottom panel of Fig. 2, and it describes the fact that, though n and $n+2$ bps are not nearest neighbors (but are separated by the intervening $n+1$ bp), they are exactly located in front of each other along the helix axis. As a consequence, the distance between the bps labeled 1–3, 4–6 or 7–9 (measured along the helix axis, namely, $2h_d\simeq 0.480$ nm) is *shorter* than that corresponding to their respective *nearest* neighbors, say 1–2, 2–3, 4–5, 5–6, 7–8, and 8–9, (which is measured along the backbone instead and amounts to $d=l_0/\sqrt{2}\simeq 0.499$ nm). Since the orbital overlapping is entirely determined by the distances between the nucleobases' π orbitals, it results that the π-π overlapping between next nearest-neighbors n and $n+2$ bps is favored over that corresponding to contiguous n

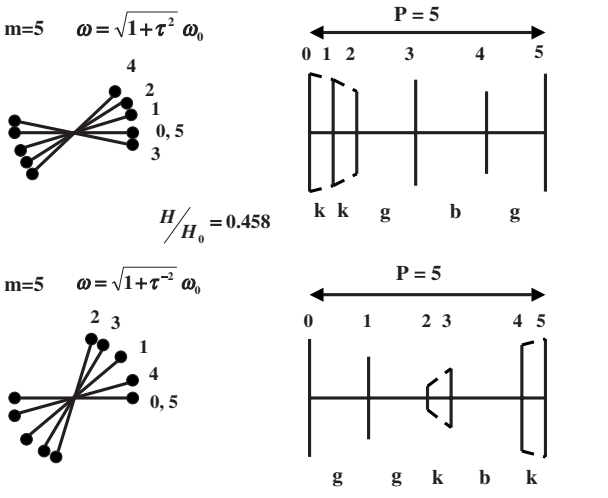

FIG. 4. The same as Figs. 2 and 3 for the frequencies $\omega_5^{\pm}=\sqrt{1+\tau^{\pm 2}}\omega_0$ for the resonance correlation length $m=5$. For more details see the text.

and $n\pm 1$ bps in this case.[49] In this way, the phyllotactic pattern related to the ω_3^+ frequency provides a representative physical instance of the geometrical configuration sketched in Fig. 1(a).

The same π-π overlapping enhancement due to helical configuration effects takes place between the bps labeled 2–4 (alternatively, 0–2) for the standing waves related to the frequency ω_4^+ (alternatively, ω_4^-), as it is illustrated in the top panel of Fig. 3. In this case, the axial distance between n and $n+2$ bps is $2h_e\simeq 0.368$ nm, whereas the backbone distance between contiguous bps is $d=l_0\sqrt{\frac{2-\sqrt{2}}{2}}\simeq 0.382$ nm. As we see, the bps forming the trimer 2–3–4 (alternatively, 0–1–2) are closely packed, while those forming the trimer 0–1–2 (alternatively, 2–3–4) are broadly distributed instead. Such a succession of alternating tight- and broad-packed trimers is necessary to preserve the mechanical stability of the duplex chain over long distances. Two additional features of the standing waves related to the resonance correlation length $m=4$ are: (i) the spatial period of the corresponding standing wave is significantly reduced ($P=4$ bps, $H/H_0=0.369$) with respect to the H/H_0 value obtained for the frequency ω_3^+; and (ii) the arrangement of nucleobases along the backbone (i.e., the phyllotactic pattern) for the standing wave corresponding to the ω_4^+ frequency is related to that corresponding to the ω_4^- frequency by means of a *mirror-symmetry* operation with respect to a sagittal plane containing the even numbered bps (see Fig. 3, top panel). An analogous symmetry property (now including a permutation affecting 1 and 3–4 bps) is observed in the phyllotactic patterns related to the helical standing waves corresponding to the frequencies $\tau^{\pm 1}\omega_0$ (see Fig. 3, bottom panel), though the spatial period of the related standing waves ($P=5$ bps, $H/H_0=0.435$) is longer than that of the $\omega_4^{\pm}$ frequency related ones. Consequently, the tight-packed 0–1–2 (alternatively, 2–3–4–5) bp units extend over a longer axial distance ($2h_h=0.566$ nm) than the previously considered standing waves, which implies a less pronounced π-π overlapping enhancement effect (by inspecting Table III we have $h<d<e$). Finally, let us consider the helical configurations corresponding to the $m=5$ resonance correlation length for the frequencies $\sqrt{1+\tau^{\pm 2}}\omega_0$ shown in Fig. 4. In this case the period of the standing waves ($P=5$ bps, $H/H_0=0.458$) is somewhat longer than that obtained for the frequencies $\tau^{\pm 1}\omega_0$, though the most relevant feature is that we obtain a more complex phyllotactic pattern than the previously considered ones. In fact, three different transfer coupling values are now present, one of them ($k=0.117$ eV) describing the largest π-π overlapping value listed in Table IV. On the other hand, the phyllotactic pattern corresponding to the $\sqrt{1+\tau^2}\omega_0$ frequency related standing wave remarkably differs from that related to the $\sqrt{1+\tau^{-2}}\omega_0$ frequency one. In the former case, we have *three* consecutive bps (namely, 0–1–2) strongly interacting with each other, whereas in the later case we only have interacting dimers (namely, 2–3 and 4–5) instead. In addition, the relative orientation of the strongly interacting units considerably differs in both cases.

IV. TWIST PHONON COUPLING EFFECTS ON THE ENERGY SPECTRA

In Sec. III we have learnt that each resonance frequency is related to a helical standing wave determining a characteris-

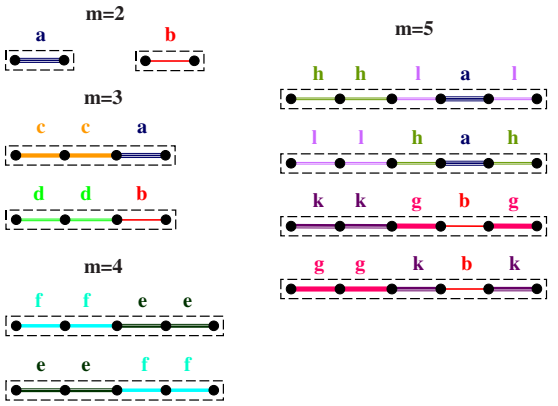

FIG. 5. (Color online) Effective one-dimensional lattice unit cells corresponding to the different π-π overlapping resonance configurations of duplex DNA for correlation length values $m=2-5$. The values of the different transfer integrals labeled in the figure are listed in Tables III and IV. For more details see the text.

tic geometrical configuration of the duplex DNA. The corresponding helical patterns exhibit a shortened spatial period along the helix axis, as compared to that corresponding to the equilibrium configuration. This stretching originates a local rearrangement of bps which properly group into alternating series of either compressed or elongated dimer or trimer blocks of bps units (in order to preserve the mechanical stability of the whole DNA chain). This geometrical arrangement, in turn, determines a series of possible values for the transfer integrals describing the π-π overlapping between closer bps. In this way, the effective DNA unit cells stemming from twist phonon coupling effects will play a significant role in the resulting electronic structure properties and we will obtain a characteristic band structure for every resonance frequency.

In this section we will perform a systematic study on the influence of this phonon coupling effect on the electronic structure of duplex DNA chains. To this end, one can usefully exploit the simple mathematical structure of Eq. (12) in order to use the standard transfer-matrix techniques to properly analyze a fully three-dimensional, realistic model of duplex DNA. By expressing Eq. (12) in the matrix form

$$\begin{pmatrix} \psi_{n+1} \\ \psi_n \end{pmatrix} = \begin{pmatrix} \dfrac{E-\tilde{\varepsilon}_n(E)}{\tilde{\tau}_{n,n+1}(\omega)} & -\dfrac{\tilde{\tau}_{n,n-1}(\omega)}{\tilde{\tau}_{n,n+1}(\omega)} \\ 1 & 0 \end{pmatrix} \begin{pmatrix} \psi_n \\ \psi_{n-1} \end{pmatrix}, \quad (19)$$

the dispersion relation corresponding to a chain of length N can be obtained from expression

$$\cos(qNl_0) = \frac{1}{2}\mathrm{tr}[\mathcal{M}_N(E,\omega)] = \frac{1}{2}\mathrm{tr}\left[\prod_{n=N}^{1} M_n(E,\omega)\right], \quad (20)$$

where the local transfer matrices $M_n(E,\omega)$ are given by Eq. (19). According to Eq. (13) for each resonance frequency value we get a specific distribution pattern of transfer integrals along the chain. For the sake of simplicity, in this work we shall restrict ourselves to the study of homopolymer sys-

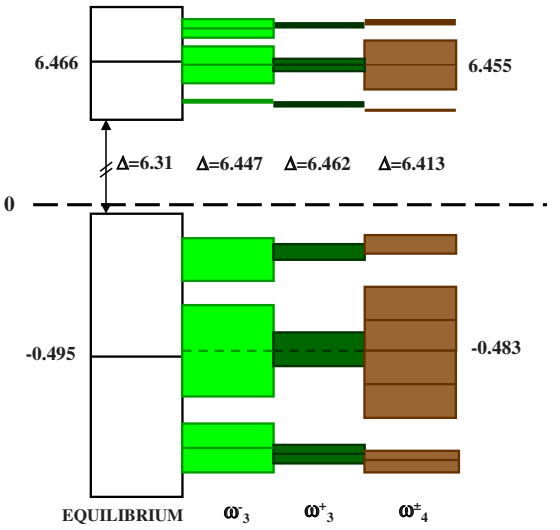

FIG. 6. (Color online) Electronic energy spectra for several resonance frequencies are compared to that corresponding to the equilibrium B-DNA form of polyG-polyC. The numbers indicate energy values (in eV).

tems (i.e., synthetic polyG-polyC or polyA-polyT chains), so that all the on-site energies given by Eq. (2) take on the same value. In so doing, the limelight is cast onto lattice coupling effects rather than on the chemical diversity characteristic of typical biological DNA samples, where four different nucleotides are aperiodically distributed along the chain.[50] Thus, the transfer integrals pattern distributions corresponding to the correlation lengths $m=1$ and $m=2$ are simply described in terms of a monatomic, one-dimensional effective lattice model. For $m \geq 3$ the resulting $\tilde{\tau}_{n,n\pm1}(\omega)$ distributions result in richer lattice models, characterized by progressively larger unit cells, as it is illustrated in Fig. 5. As expected, both the number of possible $\tilde{\tau}_{n,n\pm1}(\omega)$ values and the complexity of the effective lattice unit cell progressively increases as m increases. Making use of Eq. (20) one obtains the dispersion relations listed in Table V, where we have introduced the auxiliary variable $u \equiv E-\alpha(E)$ (alternatively, $u \equiv E-\beta(E)$ for polyA-polyT chains). The corresponding energy spectra are plotted in Figs. 6 and 7 and relevant information about the electronic structure is listed in Tables VI and VII. The spectra have been derived from the dispersion relations listed in Table V, making use of the model parameters and transfer integral values listed in Tables I and III, respectively. The overall structure of these spectra consists of two regions of allowed energy bands separated by a relatively broad gap of about $\Delta=6.3-6.4$ eV width. The high energy region of the spectra, located around the energy value $E \simeq 6.46$ eV, is related to the sugar-phosphate DNA subsystem, whereas the low energy region, centered around the value $E \simeq -0.49$ eV, is related to the nucleobase DNA subsystem.[43,51] In the equilibrium configuration the electronic spectrum is composed of two relatively broad bands. Due to the lattice coupling effects, both bands are split in a number of narrower subbands. The number of the resulting subbands is given by the resonance correlation length value, m. Accordingly, the longer the correlation length, the larger the fragmentation degree of the electronic spectrum due to vibrational effects. The pres-

TABLE V. Dispersion relations given by Eq. (20) for the unit cells corresponding to the π-π overlapping correlation lengths $m=1-5$ (see Fig. 5). The different possible values of the transfer integrals $\tau_j \equiv \tilde{\tau}_{n,n+1}(\omega)$ for a given unit cell are listed in Table III. $B' \equiv \frac{6\tau_{j_1}^2+3\tau_{j_2}^2+\tau_{j_3}^2}{\sqrt[3]{A}}$ and $A=4\tau_{j_3}(-36\tau_{j_1}^2+9\tau_{j_2}^2+2\tau_{j_3}^2)+12i\sqrt{3}\sqrt{8\tau_{j_1}^2(4\tau_{j_1}^4+6\tau_{j_1}^2\tau_{j_2}^2-4\tau_{j_1}^2\tau_{j_3}^2+3\tau_{j_2}^4+5\tau_{j_2}^2\tau_{j_3}^2+\tau_{j_3}^4)+\tau_{j_2}^4(\tau_{j_3}^2-4\tau_{j_2}^2)}$. For more details see the text.

m	Dispersion relation	τ_j	ω/ω_0	Band edges
1, 2	$u=2\tau\cos(ql_0)$	$a/b/\tau_0$	$2,0,\sqrt{2}$	$u=\pm 2\tau_j$
3	$u^3-u(\tau_2^2+2\tau_1^2)=2\tau_1^2\tau_2\cos(3ql_0)$	$c\ a$ $d\ b$	1 $\sqrt{3}$	$u=-\tau_{j_2}$ $u=\frac{\tau_{j_2}\pm\sqrt{\tau_{j_2}^2+8\tau_{j_1}^2}}{2}$
				$u=\tau_{j_2}$ $u=\frac{-\tau_{j_2}\pm\sqrt{\tau_{j_2}^2+8\tau_{j_1}^2}}{2}$
4	$u^4-2u^2(\tau_2^2+\tau_1^2)+2\tau_1^2\tau_2^2=2\tau_1^2\tau_2^2\cos(4ql_0)$	e,f	$\sqrt{2\pm\sqrt{2}}$	$u=0,\ u=\pm\sqrt{2(\tau_{j_2}^2+\tau_{j_1}^2)}$
				$u=\pm\sqrt{2}\tau_{j_1},\ \pm\sqrt{2}\tau_{j_2}$
5	$u[u^4-u^2(\tau_3^2+2\tau_2^2+2\tau_1^2)+2\tau_1^2(\tau_3^2+\tau_2^2)+\tau_2^4]$ $=2\tau_1^2\tau_2^2\tau_3\cos(5ql_0)$	$h\ l\ a$ $k\ g\ b$	$\tau^{\pm 1}$ $\sqrt{1+\tau^{\pm 2}}$	$u=-\frac{\tau_{j_3}}{2}\pm\frac{1}{2}\sqrt{\tau_{j_3}^2+4\tau_{j_2}^2}$ $u=\frac{\sqrt[3]{A}+4B'+2\tau_{j_3}}{6}$ $u=-\frac{\sqrt[3]{A}+4B'-4\tau_{j_3}\pm i\sqrt{3}(\sqrt[3]{A}-4B')}{12}$
				$u=\frac{\tau_{j_3}}{2}\pm\frac{1}{2}\sqrt{\tau_{j_3}^2+4\tau_{j_2}^2}$ $u=\frac{\sqrt[3]{A}+4B'-2\tau_{j_3}}{6}$ $u=-\frac{\sqrt[3]{A}+4B'+4\tau_{j_3}\pm i\sqrt{3}(\sqrt[3]{A}-4B')}{12}$

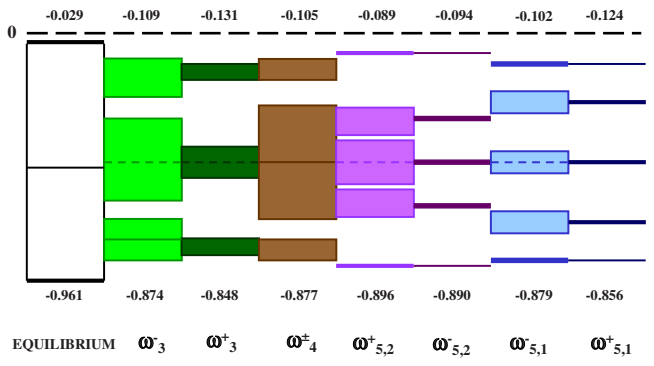

FIG. 7. (Color online) Electronic energy spectra for several resonance frequencies are compared to that corresponding to the equilibrium B-DNA form of polyG-polyC in the energy window close to the Guanine on-site energy (energy reference value). The numbers indicate the energy values (in eV) of the top and bottom edges of the spectra.

ence of these subbands should not be regarded as indicating a purely bandlike transport mechanism, since the subbands closer to the Fermi level are too narrow to play the major role in charge transport. In addition, we observe that: (i) the value of the main gap between the top of the valence band and the bottom of the conduction band slightly increases as a consequence of the fragmentation from $\Delta=6.31$ eV (equilibrium configuration) to $\Delta\simeq 6.45$ eV ($m=3$), $\Delta=6.41$ ($m=4$), and $\Delta\simeq 6.45$ eV ($m=5$), and (ii) the distance between the top of the valence band and the Fermi level also increases ($0.09\lesssim\delta\lesssim 0.12$ eV) as compared to the equilibrium configuration value ($\delta\simeq 0.03$ eV) due to dynamical effects. Thus, twist coupled, π-π overlapping resonance effects do not significantly improve charge-transport efficiency, though the orchestrated nature of the helical waves propagating along the DNA prevents the conductivity degradation which will occur in the presence of incoherent thermal fluctuations alone.

The overall electronic band structure is not qualitatively affected by the choice of the transfer integral value in a

TABLE VI. Allowed bands locations (E_i) and bandwidths (W_i) in the energy spectrum of a polyG-polyC duplex for the resonance frequencies corresponding to the correlation lengths $m=2-4$.

Band center (eV)	ω_-	ω_+	Bandwidth (meV)	ω_-	ω_+
		$m=2$			
E_1	−0.503	−0.495	W_1	1212	931
E_2	+6.475	+6.466	W_2	478	366
		$m=3$			
	ω_3^-	ω_3^+		ω_3^-	ω_3^+
E_1	−0.796	−0.820	W_1	155	57
E_2	−0.484	−0.483	W_2	300	109
E_3	−0.181	−0.158	W_3	145	53
E_4	+6.339	+6.330	W_4	54	20
E_5	+6.455	+6.454	W_5	118	43
E_6	+6.581	+6.590	W_6	64	24
		$m=4$			
	$\omega_4^\pm$			$\omega_4^\pm$	
E_1	−0.842		W_1	70	
E_2	−0.593		W_2	221	
E_3	−0.375		W_3	216	
E_4	−0.138		W_4	65	
E_5	+6.309		W_5	3	
E_6	+6.412		W_6	83	
E_7	+6.498		W_7	88	
E_8	+6.599		W_8	29	

significant way. The value $t_0=0.15$ eV listed in Table I is about twice the average value $\langle t\rangle=0.07$ eV describing the intrastrand coupling of purine nucleobases, as derived from quantum mechanical-molecular dynamics calculations.[10] Keeping in mind the wide fluctuations of this coupling around its mean value,[5–9] the adopted t_0 can be regarded as a quite representative one, small enough as compared to the optimal transfer integral value $t_*=0.37$ eV establishing the maximum physically acceptable value for this parameter. We have checked that the width of the different bands in the electronic spectrum linearly scales with the transfer integral value within the interval $\langle t\rangle \leq t \leq t_*$. For the sake of illustration in Table VIII we list the bandwidth dependence on the adopted t_0 value for the lower energy spectrum region corresponding to the frequencies $\omega_3^\pm$. By inspecting this table we see that most bandwidths are wider enough to be of physical

TABLE VII. Allowed bands locations (E_i) and bandwidths (W_i) in the energy spectrum of a polyG-polyC duplex for the resonance frequencies corresponding to the correlation length $m=5$.

Band center (eV)	$\omega_{5,2}^+$	$\omega_{5,2}^-$	$\omega_{5,1}^-$	$\omega_{5,1}^+$	Bandwidth (meV)	$\omega_{5,2}^+$	$\omega_{5,2}^-$	$\omega_{5,1}^-$	$\omega_{5,1}^+$
E_1	−0.887	−0.888	−0.849	−0.852	W_1	15	4	31	7
E_2	−0.638	−0.655	−0.720	−0.720	W_2	101	19	73	17
E_3	−0.483	−0.483	−0.483	−0.483	W_3	170	30	81	19
E_4	−0.331	−0.314	−0.252	−0.252	W_4	97	18	69	16
E_5	−0.096	−0.096	−0.131	−0.128	W_5	13	3	29	7
E_6	+6.307	+6.307	+6.320	+6.319	W_6	5	1	11	3
E_7	+6.395	+6.389	+6.365	+6.365	W_7	37	7	26	6
E_8	+6.454	+6.454	+6.454	+6.454	W_8	67	12	32	7
E_9	+6.516	+6.523	+6.549	+6.549	W_9	41	8	30	7
E_{10}	+6.618	+6.619	+6.602	+6.604	W_{10}	6	2	13	3

TABLE VIII. Dependence of the low energy bandwidths [W_i in (meV)] on the adopted transfer integral value t (in eV) in the energy spectrum of a polyG-polyC duplex for the resonance frequencies $\omega_3^{\pm}$.

ω_3^- bandwidth	$t=0.07$	$t=0.15$	$t=0.30$
W_1	71	155	319
W_2	140	300	599
W_3	70	145	277
ω_3^+ bandwidth	$t=0.07$	$t=0.15$	$t=0.30$
W_1	26	57	117
W_2	51	109	219
W_3	25	53	100

significance as compared to typical vibrational energy scales within the range 10–25 meV.

Finally, we note that the time scale corresponding to the resonance frequencies (see Table III) spans from $T \simeq 5.1$ ps (for $\omega_{5,1}^-$) to $T \simeq 15.9$ ps (for $\omega_{5,1}^+$), reasonably fitting the characteristic 5–10 ps decay process time constant previously reported from spectroscopy experiments.[22,23] Accordingly, the time period of the standing waves related to the collective twist motion of the bps and the experimentally determined charge-transfer rates occur on comparable time scales. This result is in line with detailed numerical analysis on the kinetics of charge transfer in donor-bridge-acceptor systems in which electronic coupling can fluctuate in time due to the torsional motion of adjacent structural units relative to each other.[7]

V. CONCLUSIONS

In this work we report on the emergence of helicoidal standing waves in the DNA duplex due to synchronized, collective twist motions of the bps which can efficiently enhance the π-π orbital overlapping between *nonconsecutive* bps via a long-range, phonon-correlated tunneling effect. The resulting structural patterns can be described within the framework of dynamical phyllotaxis, so that for every standing wave characterized by its resonance frequency, we obtain a specific *DNA phyllotactic pattern*, describing the helical arrangement of the nucleobases along the duplex chain.

To this end, we have expressed charge-lattice interaction in terms of nearest-neighbor tight-binding equations describing the propagation of the charge through an effective linear lattice for certain frequency values, providing a realistic treatment which takes into account both the intrinsic three-dimensional, helicoidal geometry of DNA, and the coupling between the electronic degrees of freedom and duplex DNA (low frequency) molecular dynamics. The corresponding effective transfer integrals include both helicoidal and dynamical effects in an intertwined fashion, allowing for a unified treatment of charge-lattice coupled dynamics in a fully analytical way in terms of Chebyshev polynomials.

In this way, we disclose the relationship between a number of π-π overlapping resonance frequencies and the main features of the resulting DNA electronic band structure. A remarkable result regarding twist motion effects is that we can assign a *characteristic electronic structure* to each resonance frequency. Since these frequencies also determine a series of possible DNA configurations stemming from certain helical standing-waves patterns, we have the possibility of assigning such conformational structures to the electronic structure of the DNA chain in a direct and precise way. Such a link could have far-reaching consequences in order to relate electronic properties of nucleic acids to shape recognition processes of metabolic interest (v. g., protein-DNA binding) at a molecular scale.[51,52]

Another remarkable feature is that the fragmented nature of the energy spectrum gives rise to the presence of *two* different *energy scales* in the DNA band structure due to the main band fragmentation induced via twist coupling. Thus, we have a large energy scale (within the range ~6.5 eV) determined by the width of the wide gap among the main bands, respectively, related to the nucleobases and sugar-phosphate subsystems. In addition, we also have a small energy scale (ranging from about 0.25–0.02 eV) related to the presence of several narrow gaps in the spectra of resonant helical modes. The presence of these small activation energies in the electronic structure brings an additional mechanism in order to explain the anomalous absorption feature observed at low (10–100 meV) energies in optical conductivity spectra of biological DNA samples.[53,54]

Some words regarding the possible effect of the water-counterions surrounding on the collective twist motion of bps are in order. Broadly speaking these effects are twofold. On the one hand, both the on-site energies and the transfer integrals values could be changed as a consequence of the interaction of the sugar-phosphate and nucleobase subsystems with water molecules. On the other hand, viscous damping effects along with an enhancement of the bp effective mass should be introduced in the lattice Hamiltonian. According to detailed quantum chemical-molecular dynamics calculations the fluctuation of counterions are strongly counterbalanced by the surrounding water, leading to large oscillations of the on-site energies. In contrast, the transfer integral couplings depend only on DNA conformation and are not significantly affected by the solvent.[21] Therefore, one should not expected a relevant influence of the environment on the reported bandwidths, which are mainly determined by the transfer integral values, though the precise location of the bands would be probably affected by the on-site energy modulation. Within our adopted approach such a modulation could be readily incorporated into the renormalized on-site energies describing the Watson-Crick energetics given by Eq. (2). In fact, the study of a possible competition between on-site energy fluctuations arising from environmental effects (favoring localization of charge) and the existence of off-diagonal correlations in the electronic Hamiltonian stemming from the π-π orbital overlapping mechanism presented in this work would be a very appealing issue deserving further study, particularly in the light of the recent results reporting on the crucial role of correlated fluctuations of the bps dynamics in the Landauer conductance of DNA chains.[55] Regarding the lattice Hamiltonian one expects that damping effects are not very important, particularly for chains con-

taining less than 10^3 bps.[56] Thus, the main dynamical effect on the collective twist motion is expected to arise from the effective-mass enhancement of the bps, leading to a relative increase in the resonance frequencies by just a few percent.

As a final remark we note that most quasiperiodic systems also exhibit highly fragmented, fractal-like energy spectra.[41] In the case of DNA chains grown according to the Fibonacci sequence, the main features of the fragmentation pattern have been ascribed to the presence of long-range spatial correlations of nucleobases under static conditions.[57] Thus, the analysis of possible competing effects between energy spectra fragmentation schemes arising from an aperiodic distribution of on-site energies in the nucleobase subsystem, on the one hand, and fragmentation patterns stemming from charge-lattice coupling dynamical effects in synthetic Fibonacci DNA, on the other hand, would be a very appealing issue to be considered in a forthcoming extension of this work.

ACKNOWLEDGMENTS

I warmly thank Alexander Voityuk for sharing useful information and M. V. Hernández for a critical reading of the manuscript. This work has been supported by the Universidad Complutense de Madrid and Banco Santander through Project No. PR34/07-15824.

[1] D. Beeker, A. Adhikary, and M. D. Sevilla, in *Charge Migration in DNA. Perspectives from Physics, Chemistry and Biology*, edited by T. Chakraborty (Springer, Berlin, 2007), p. 139.
[2] E. Braun, Y. Eichen, U. Sivan, and G. Ben-Yoseph, Nature (London) **391**, 775 (1998).
[3] C. R. Treadway, M. G. Hill, and J. K. Barton, Chem. Phys. **281**, 409 (2002).
[4] R. G. Endres, D. L. Cox, and R. R. P. Singh, Rev. Mod. Phys. **76**, 195 (2004).
[5] A. A. Voityuk, J. Chem. Phys. **128**, 045104 (2008).
[6] A. A. Voityuk, K. Siriwong, and N. Rösch, Phys. Chem. Chem. Phys. **3**, 5421 (2001).
[7] Y. A. Berlin, F. C. Grozema, L. D. A. Siebbeles, and M. A. Ratner, J. Phys. Chem. C **112**, 10988 (2008).
[8] Y. A. Berlin, I. V. Kurnikov, D. Beratan, M. A. Ratner, and A. L. Burin, in *DNA Electron Transfer Processes: Some Theoretical Notions*, edited by G. B. Schuster (Springer, Berlin, 2004), p. 1.
[9] A. Troisi and G. Orlandi, J. Phys. Chem. B **106**, 2093 (2002).
[10] A. A. Voityuk, J. Chem. Phys. **128**, 115101 (2008).
[11] A. A. Voityuk, J. Jortner, M. Bixon, and N. Rösch, J. Chem. Phys. **114**, 5614 (2001); A. A. Voityuk, Chem. Phys. Lett. **439**, 162 (2007).
[12] P. J. de Pablo, F. Moreno-Herrero, J. Colchero, J. Gomez Herrero, P. Herrero, A. M. Baro, P. Ordejón, J. M. Soler, and E. Artacho, Phys. Rev. Lett. **85**, 4992 (2000).
[13] R. Di Felice, A. Calzolari, E. Molinari, and A. Garbesi, Phys. Rev. B **65**, 045104 (2001).
[14] H. Wang, J. P. Lewis, and O. F. Sankey, Phys. Rev. Lett. **93**, 016401 (2004).
[15] Y. A. Berlin, M. L. Burin, and M. A. Ratner, Superlattices Microstruct. **28**, 241 (2000).
[16] E. Artacho, M. Machado, D. Sánchez-Portal, P. Ordejón, and J. M. Soler, Mol. Phys. **101**, 1587 (2003).
[17] H. Sugiyama and I. Saito, J. Am. Chem. Soc. **118**, 7063 (1996).
[18] E. B. Starikov, Philos. Mag. **85**, 3435 (2005).
[19] K. Senthilkumar, F. C. Grozema, C. Fonseca Guerra, F. M. Bickelhaupt, F. D. Lewis, Y. A. Berlin, M. A. Ratner, and L. D. A. Siebbeles, J. Am. Chem. Soc. **127**, 14894 (2005).
[20] F. C. Grozema and L. D. A. Siebbeles, in *Charge Migration in DNA. Perspectives from Physics, Chemistry and Biology* (Ref. 1), p. 21.
[21] T. Kubar and M. Elstner, J. Phys. Chem. B **112**, 8788 (2008).
[22] C. Wan, T. Fiebig, S. O. Kelley, C. R. Treadway, J. K. Barton, and A. H. Zewail, Proc. Natl. Acad. Sci. U.S.A. **96**, 6014 (1999).
[23] C. Wan, T. Fiebig, O. Schiemann, J. K. Barton, and A. H. Zewail, Proc. Natl. Acad. Sci. U.S.A. **97**, 14052 (2000).
[24] Y. Duan, P. Wilkosz, M. Crowley, and J. Rosenberg, J. Mol. Biol. **272**, 553 (1997).
[25] S. Roche, Phys. Rev. Lett. **91**, 108101 (2003).
[26] Y. Zhu, C. C. Kaun, and H. Guo, Phys. Rev. B **69**, 245112 (2004).
[27] W. Ren, J. Wang, Z. Ma, and H. Guo, Phys. Rev. B **72**, 035456 (2005); J. Chem. Phys. **125**, 164704 (2006).
[28] A.-M. Guo and H. Xu, Physica B **391**, 292 (2007).
[29] R. Gutiérrez, S. Mandal, and G. Cuniberti, Phys. Rev. B **71**, 235116 (2005).
[30] R. Gutiérrez, S. Mohapatra, H. Cohen, D. Porath, and G. Cuniberti, Phys. Rev. B **74**, 235105 (2006).
[31] G. Cuniberti, E. Maciá, A. Rodríguez and R. A. Römer, in *Charge Migration in DNA. Perspectives from Physics, Chemistry and Biology* (Ref. 1), p. 1.
[32] E. Maciá, Phys. Rev. B **76**, 245123 (2007).
[33] J. P. Lewis, Th. E. Cheatham III, E. B. Starikov, H. Wang, and O. F. Sankey, J. Phys. Chem. B **107**, 2581 (2003).
[34] C. J. Paez and P. A. Shulz, Microelectron. J. **39**, 1222 (2008).
[35] Phyllotaxis refers to the geometrical ordering of certain botanical elements, like leaves or flowers, on the stem of a plant. The interested reader is referred to the classical works: I. Adler, J. Theor. Biol. **45**, 1 (1974); **53**, 435 (1975); **65**, 29 (1977); G. J. Mitchison, Science **196**, 270 (1977); R. V. Jean, *Phyllotaxis: A Systemic Study in Plant Morphogenesis* (Cambridge University Press, Cambridge, 1994).
[36] N. Rivier, R. Occelli, J. Pantaloni, and A. J. Lissowski, J. Phys. (France) **45**, 49 (1984).
[37] L. S. Levitov, Phys. Rev. Lett. **66**, 224 (1991); EPL **14**, 533 (1991).
[38] S. Douady and Y. Couder, Phys. Rev. Lett. **68**, 2098 (1992).
[39] E. Maciá, Z. Kristallogr. **224**, 91 (2009).
[40] E. Maciá, Rep. Prog. Phys. **69**, 397 (2006).
[41] E. Maciá, *Aperiodic Structures in Condensed Matter: Fundamentals and Applications* (CRC Press, Boca Raton, FL, 2009).
[42] E. Maciá and S. Roche, Nanotechnology **17**, 3002 (2006).
[43] E. Maciá, Phys. Rev. B **74**, 245105 (2006); **75**, 035130 (2007).

[44] Z. G. Yu and X. Song, Phys. Rev. Lett. **86**, 6018 (2001).
[45] W. Zhang, A. O. Govorov, and S. E. Ulloa, Phys. Rev. B **66**, 060303(R) (2002).
[46] S. Cocco and R. Monasson, Phys. Rev. Lett. **83**, 5178 (1999); J. Chem. Phys. **112**, 10017 (2000).
[47] R. Endres, D. Cox, and R. Singh, arXiv:cond-mat/0201404 (unpublished).
[48] Note that the adopted μ value coincides with the averaged mass of the four nucleotides, i.e., $\mu \simeq (m_G+m_C+m_A+m_T)/4$.
[49] A similar effect, involving dipolar magnetic interactions among magnets arranged in a helicoidal manner has been recently reported by C. Nisoli, N. M. Gabor, P. E. Lammert, J. D. Maynard, and V. H. Crespi, Phys. Rev. Lett. **102**, 186103 (2009).
[50] This interesting issue will be addressed elsewhere.
[51] J. Ladik, A. Bende, and F. Bogár, J. Chem. Phys. **128**, 105101 (2008); **127**, 055102 (2007).
[52] T. J. Richmond and C. A. Davey, Nature (London) **423**, 145 (2003); K. Luger, A. W. Mäder, R. K. Richmond, D. F. Sargent, and T. J. Richmond, *ibid.* **389**, 251 (1997).
[53] A. Hübsch, R. G. Endres, D. L. Cox, and R. R. P. Singh, Phys. Rev. Lett. **94**, 178102 (2005).
[54] A. Omerzu, D. Mihailovic, B. Anzelak, and I. Turel, Phys. Rev. B **75**, 121103(R) (2007).
[55] P. B. Woiczikowski, T. Kubar, R. Gutiérrez, R. A. Caetano, G. Cuniberti, and M. Elstner, J. Chem. Phys. **130**, 215104 (2009).
[56] P. Thomen, U. Bockelmann, and F. Heslot, Phys. Rev. Lett. **88**, 248102 (2002).
[57] S. Roche, D. Bicout, E. Maciá, and E. Kats, Phys. Rev. Lett. **91**, 228101 (2003).